Clays and Clay Minerals, Vol. 64, No. 4, 337–347, 2016.

CADMIUM(II) COMPLEXES ADSORBED ON CLAY EDGE SURFACES: INSIGHT FROM FIRST PRINCIPLES MOLECULAR DYNAMICS SIMULATION

Chi Zhang[1], Xiandong Liu[1,*], Xiancai Lu[1], Evert Jan Meijer[2], Kai Wang[1], Mengjia He[1], and Rucheng Wang[1]

[1] State Key Laboratory for Mineral Deposits Research, School of Earth Sciences and Engineering, Nanjing University, Nanjing 210093, P.R. China

[2] Van't Hoff Institute for Molecular Sciences and Amsterdam Center for Multiscale Modeling, University of Amsterdam, Science Park 904, 1098 XH, Amsterdam, The Netherlands

Abstract—Aiming to identify the complexing mechanisms of heavy metal cations on edge surfaces of 2:1-type clay minerals, systemic first-principles molecular dynamics (FPMD) simulations were conducted and the microscopic structures and complex free energies were obtained. Taking Cd(II) as a model cation, the structures on both (010) and (110) edges of the complexes were derived for the three possible binding sites ($\equiv$SiO, $\equiv$Al(OH)$_2$/$\equiv$AlOH$\equiv$AlSiO, and vacant sites). The stable complexes adsorbed on the three binding sites on both terminations had similar structures. The free energies of the complexes on (010) edges were calculated by using the constrained FPMD method. The free energies of complexes on the $\equiv$SiO and $\equiv$Al(OH)$_2$ sites were similar and they were both significantly lower than the free energy of the complex on the octahedral vacant site. In association with the concept of high energy site (HES) and low energy site (LES) in the 2 Site Protolysis Non Electrostatic Surface Complexation and Cation Exchange (2SPNE SC/CE) sorption model, the vacant site was assigned to HES and the other two sites to LES, respectively.

Key Words—Binding Site, Cadmium Cation, Complexation, Edge Surface, First-Principles Molecular Dynamics, Free Energy.

INTRODUCTION

Clay minerals are ubiquitous in soils, sediments, and aquifers (Bergaya and Lagaly, 2013), and play important roles in transport and fixation of toxic heavy metal cations in the environment through adsorption (Evans, 1989; Sposito *et al*., 1999). This interfacial behavior has attracted significant attention in geology and environmental science (Gu and Evans, 2008; Yuan *et al*., 2013) because it greatly dominates the retention and bioavailability of heavy metals in various environments.

The 2:1-type phyllosilicates, such as smectites and vermiculites, possess large surface areas, porosities, and swelling properties (Mooney *et al*., 1952). These clay materials are widely used as adsorbent materials to fix heavy metal pollutants (Yuan *et al*., 2013) in environmental engineering. These minerals can also be applied as back fill materials in geologic disposal sites of nuclear wastes (Jo *et al*., 2006; Wagner, 2013).

The interfacial chemistry of clay minerals is complex due to the special surface structures. The layer of 2:1-type clay minerals consists of an octahedral sheet (O-sheet) sandwiched by two tetrahedral sheets (T-sheet) (Brindley and Brown, 1980). Because of the layered structures, the surfaces of these silicates are usually subdivided into basal surfaces (*i.e.* interlayer surfaces) and edge surfaces (*i.e.* broken surfaces such as (010) and (110)) (White and Zelazny, 1988; Schoonheydt and Johnston, 2013). The basal surfaces of layered silicates carry permanent negative structural charges, which are generated by isomorphic substitutions of structural cations by cations with lower valence (*i.e.*, Mg for Al replacement in O-sheets and Al for Si replacement in T-sheets). The negative charges are compensated by the interlayer cations which can exchange with dissolved solutes (Gaines and Thomas, 1953; Brigatti *et al*., 2013). In contrast to basal surfaces, edge surfaces normally have more complex structures and more subtle chemical properties due to the dangling bonds which make edge surfaces amphoteric (Bleam, 1993; Lagaly and Dékány, 2013).

Extensive adsorption experiments have been carried out to investigate the complexes of heavy metal cations on clay surfaces (Baeyens and Bradbury, 1997; Bradbury and Baeyens, 1997, 1999; Barbier *et al*., 2000; Ikhsan *et al*., 2005; Gu and Evans, 2008; Gu *et al*., 2010; Dähn *et al*., 2011). Previous studies have shown two adsorption stages as pH increases: cation exchange at permanently charged basal surfaces and the formation of complexes on edge surfaces (see, e.g., Gaines and Thomas,1953;

* E-mail address of corresponding author:
xiandongliu@nju.edu.cn
DOI: 10.1346/CCMN.2016.0640402

This paper is published as part of a special issue on the subject of 'Computational Molecular Modeling'. Some of the papers were presented during the 2015 Clay Minerals Society-Euroclay Conference held in Edinburgh, UK.

https://doi.org/10.1346/CCMN.2016.0640402 Published online by Cambridge University Press

Sposito, 1984; Baeyens and Bradbury, 1997). At low pH, cation adsorption is pH independent and corresponds to the cation exchange capacity (CEC) of interlayers. Many studies have been carried out to investigate the structures and properties of basal/interlayer surfaces (Boek and Sprik, 2003; Liu and Lu, 2006; Liu *et al*., 2008; Cygan *et al*., 2009; Anderson *et al*., 2010). The process and capacity of cation exchange are recognized to be dominated by the layer charge density of clay minerals. The complexing of edge sites is remarkably pH dependent. With pH values between 6 and 8, the amount adsorbed drastically increases and is believed to be due to inner-sphere complexes on edge surfaces. For example, a study using polarized X-ray absorption fine structure (P-XAFS) revealed that Ni(II) formed inner-sphere complexes located at the edges of montmorillonite particles (Dähn *et al*., 2003). Similar pH-dependent adsorption behaviors have also been found for different metal cations in previous studies. For instance, Ni(II) and Zn(II) have been demonstrated to have a similar pH-dependent behavior because the distribution ratio of sorbed Ni(II) and Zn(II) increased strongly as a function of pH (Baeyens and Bradbury, 1997). The same behavior has also been shown for edge complex of Cd(II) on smectites (Zachara *et al*., 1993). Gu *et al.* (2010) concluded that in higher pH range, inner-sphere complexes of Cu(II), Cd(II), Ni(II), Pb(II), and Zn(II) were formed at the variably charged sites on clay edges. Even so, the microscopic picture of edge complexing sites and structures were poorly documented and understood.

In the last few decades, surface complexation models (SCMs) have been successfully used in describing the adsorption of ions on clay minerals (Davis and Kent, 1990; Bradbury and Baeyens, 1997; Ikhsan *et al*., 2005; Turner *et al*., 2006; Geckeis *et al*., 2013; Tournassat *et al*., 2013; Gu *et al*., 2014). Based on many experimental observations, Bradbury and Baeyens (1997) proposed the 2 Site Protolysis Non Electrostatic Surface Complexation and Cation Exchange (2 SPNESC/CE) model to characterize the sorption of metals on montmorillonite. For the pH-dependent stage, in modeling of the sorption isotherm, Bradbury and Baeyens (1997) introduced the concept of two types of binding sites on clay edges based on the non-linearity of the sorption isotherm: high energy (or strong) sites (HES) and low energy (or weak) sites (LES). For metal cations, HES had high affinity but low site density while LES had lower affinity but higher site density than HES. Since then, this sorption model has been successfully used in a large number of studies modeling cation adsorption on phyllosilicates (Bradbury and Baeyens, 2005a, 2005b; Bradbury *et al*., 2005; Dähn *et al*., 2011; Soltermann *et al*., 2014). For instance, on the basis of this model, Bradbury and Baeyens (1999) reported modeling the sorption of Zn(II) and Ni(II) on Ca-montmorillonite. This model has also been used in surface complexation modeling of Eu(III) adsorption on Ca-montmorillonite and Na-illite (Bradbury *et al*., 2005). Recently, Soltermann *et al*. (2014) modelled Fe(II) uptake on natural montmorillonites with the 2 SPNESC/CE sorption model. Details of the edge complexes, such as adsorption sites and complexing structures were, however, still lacking, as these parameters were difficult to access by current experimental techniques.

By using extended X-ray absorption fine structure (EXAFS) measurements, Schlegel and Manceau (2013) proposed many possible sites for complexes on montmorillonite and kaolinite, such as edge-sharing and corner-sharing configurations on octahedra and tetrahedra, but these complexes were hard to distinguish. By using the 2SPNE SC/CE sorption model, Dähn *et al*. (2011) measured and modeled Zn(II) isotherm data, and their spectroscopic results of P-EXAFS indicated the existence of two distinct groups of edge binding sites, which agreed with the strong/weak site concept. By combining K-EXAFS spectra and ab initio molecular dynamics, Churakov and Dähn (2012) found that Zn(II) formed different inner-sphere complexes on clay edges and thus demonstrated the existence of two distinct types of edge surface binding sites: at low loading, Zn(II) was incorporated into the outermost trans-octahedra; and at medium loading, Zn(II) formed monodentate and bidentate inner-sphere surface complexes on the (010) and (110) edges. Up to now, however, no thermodynamic evidence has been reported regarding the adsorption strength of these different binding sites.

By combining electronic structure calculations and molecular dynamics, first-principles molecular dynamics (FPMD) simulations based on density functional theory (DFT) can accurately treat solvent and solute at the same quantum-mechanical level (Car and Parrinello, 1985). The FPMD simulation is, therefore, a powerful complement to experimental studies and has significantly promoted the research in the area of interfacial geochemistry (Tunega *et al*., 2004; Martorell *et al*., 2010; Liu *et al*., 2011, 2013a). As a theoretical method, FPMD simulation has been widely used in research on interfacial chemistry of clay mineral-water systems (Bickmore *et al*., 2003; Tunega *et al*., 2004; Boulet *et al*., 2006; Churakov, 2007; Kubicki *et al*., 2007; Cygan *et al*., 2009; Churakov and Kosakowski, 2010;; Liu *et al*., 2012a, 2012b).

Previous FPMD studies used to calculate pKa values proved that $\equiv$Si-OH and $\equiv AlOH_2$ groups were the major acidic surface sites of 2:1 phyllosilicates responsible for edge complexing of metal cations (Liu *et al*., 2013b, 2014). For the (010) edge surface, the calculated values of pKa for $\equiv SiOH$ and $\equiv Al(OH)(OH_2)$ groups were 7.0 and 8.3, respectively (Liu *et al*., 2013b). For the (110) edge surface, the pKa values for the $\equiv SiOH$ groups on the T-sheet were 8.0 and 8.3. The $\equiv AlSi(OH)$ site had a pKa of 1.7, and this indicated that the site remained deprotonated at common pHs. The pKa of $\equiv Al(OH_2)_{AlSiO}$ site was 5.5 (Liu *et al*., 2014). The common isomorphic substitution sites ($\equiv AlOH$ on the

https://doi.org/10.1346/CCMN.2016.0640402 Published online by Cambridge University Press

T-sheet and $Mg(OH_2)$ on the O-sheet), however, had extremely high pKa values, and thus all remained protonated at common pHs; hence, these were not effective complexing sites. The pKa range of edge complexing sites of 2:1 phyllosilicates was consistent with the pH range where pH-dependent adsorption occurred. By taking Fe(II) as a model cation, the inner-sphere complexes on clay edges have been simulated regarding the three possible sites, *i.e.* ≡SiO, $\equiv Al(OH)_2$, and vacant octahedral site.

To date, only a few quantum-mechanical simulations have been carried out to investigate the metal cation complexes adsorbed on the edge surfaces of clay minerals (Kremleva *et al*., 2009, 2011, 2012, 2015; Liu *et al*., 2012c; Alexandrov and Rosso, 2013). The present study aimed to provide novel understanding of the microscopic complexing structures and the adsorption mechanism of heavy metal cations on clay edges by systematic FPMD simulations. Taking Cd(II) as the model cation for its significance in geochemistry and environmental science (Zachara and Smith, 1994; Barbier *et al*., 2000; Gu *et al*., 2014), advanced FPMD simulations were carried out to calculate the desorption/adsorption free energies on the possible sites. The results indicated that the vacant site can be assigned to HES and the other two sites to LES. This study provided mechanistic insights into the complexing mechanisms of heavy metal cations on edge surfaces of clay minerals.

METHODS

Models

The model clay structure was taken from the previous studies (Liu *et al*., 2012a, 2013b), which was derived from the report of Viani *et al*. (2002). The chemical formula was $Al_4Si_8O_{20}(OH)_4$ and the crystallographic parameters were a = 5.18 Å, b = 8.98 Å, and c = 10 Å and $\alpha = \beta = \gamma = 90^o$. No isomorphic substitution was imposed in the solid part, and this model was, therefore, analogous to pyrophyllite, which is a neutral 2:1-type phyllosilicate. The models of (010) edge surfaces were cut from the unit cell and repeated along the a axis; thus two unit cells were contained in the simulated models (Figure 1).

All these surface models were placed in 3D periodically repeated orthorhombic boxes. For each box, 36 water molecules were inserted into an approximately 12 Å solution space along the direction vertical to the edge surfaces (Figure 1). This number of water molecules approximately reproduced the density of bulk water at ambient conditions.

Previous studies have shown that for Al(III) cations at (010) edge surfaces of 2:1-type phyllosilicates, both five-fold and six-fold coordination were possible and the latter was more stable (Liu *et al*., 2012a). In the present study, therefore, only six-fold cases were investigated. For the complexes, the binding sites of surface groups were initially deprotonated (*i.e.* ≡Si−O, ≡Al−OH, and ≡Al−O−Si≡), and thus the charge was +1 on all three types of Cd(II) complexes. In the CP2K/QUICKSTEP code, a background charge was added to neutralize the net charge. The Cd(II) was initially placed 2.3 Å (based on Cd−O distance of aqueous hexa-coordinated $[Cd(OH_2)_6]^{2+}$) (Rudolph and Pye, 1998; Pye *et al*., 2006) away from the binding O (*i.e.*, silanol, aluminol, or bridging site) in each model. According to the six-fold coordination scenario of Cd(II) in liquid water (Rudolph and Pye, 1998), the initial complexing configurations on the three binding sites were $\equiv SiO-Cd(H_2O)_5$,

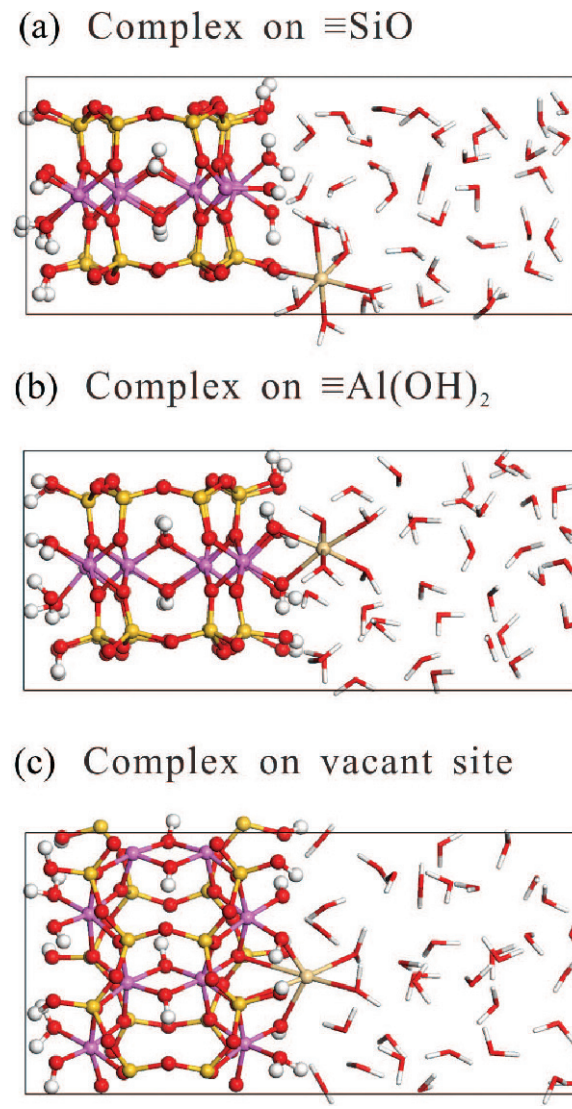


Figure 1. Models for Cd(II) complexes on three binding sites on a (010) type interface of neutral framework 2:1 phyllosilicates. (a) ≡SiO site; (b) $\equiv Al(OH)_2$ site; (c) vacant site. Solid parts and cations are shown as ball-and-stick models; solvent water molecules are shown as sticks. O = red (black), H = white (white), Al = purple (dark gray), Si = yellow (gray), and Cd = gold (light gray) with grayscale in parentheses.

https://doi.org/10.1346/CCMN.2016.0640402 Published online by Cambridge University Press

$\equiv Al(OH)_2-Cd(H_2O)_4$, and $(\equiv AlSiO \equiv AlOH)_2-Cd(H_2O)_2$, respectively.

First-principles molecular dynamics

All simulations in this work were performed with the CP2K/QUICKSTEP package (VandeVondele *et al.*, 2005). By using this code, the electronic structure was calculated with DFT implemented based on a hybrid Gaussian plane wave (GPW) approach (Lippert *et al.*, 1997). The Perdew, Burke, and Ernzerhof gradient-corrected correlation (PBE) functional (Perdew *et al.*, 1996) was used for the exchange-correlation. Goedecker-Teter-Hutter pseudopotentials (Goedecker *et al.*, 1996) were employed to describe the interactions of the core states and the valence. The double-zeta valence-polarized (DZVP) basis sets were used for H, O, Al, Si, and Cd. The plane wave basis cutoff for the electron density was set to be 280 Ry.

Born-Oppenheimer molecular dynamics (BOMD) simulations were carried out with a wave function optimization tolerance of 1.0×10^{-6} and a time step of 0.5 fs for a reasonable energy conservation. The temperature was controlled at 300 K with the Nosé-Hoover chain thermostat (Marx and Hutter, 2009). For each system, an equilibration simulation was first performed for at least 4.0 ps, and after that a production run was carried out for 5.0–15.0 ps. This was because, in the free energy calculations (see the Section 2.3), the forces of the constraint at some points reached a reasonable convergence in a simulation time of ~5.0 ps, but some other simulations needed longer durations.

Method of constraint

To fully understand and quantify the strength of Cd(II) inner-sphere complexes on different adsorption sites, a series of constrained FPMD simulations were conducted to break the Cd(II)-O bonds in each type of complex. The free energy change (ΔF) was calculated by integrating the mean force (f) along the reaction coordinate (Q) by way of the thermodynamic integration relation in equation 1 (Carter *et al.*, 1989; Sprik, 1998, 2000; Sprik and Ciccotti, 1998).

$$\Delta F(Q) = -\int_{Q_0}^{Q} dQ' f(Q') \quad (1)$$

In this study, distance and coordination number (CN) served as the Q to represent reaction processes. For the complex on the $\equiv SiO$ site, the distance between Cd(II) and the bare O of $\equiv SiO$ was selected as the Q. For the complex on the $\equiv Al(OH)_2$ site, the CN of Cd(II) with respect to the two O of $\equiv Al(OH)_2$ was selected as the Q. For the complex on the octahedral vacancy, the CN of Cd(II) with respect to the O of two adjacent $\equiv Al(OH)$ groups served as the Q.

In the simulations in which CN acted as the Q, CN was calculated by the summation formula in equation 2

$$n = \sum_i \frac{1-(r_i/r_c)^{12}}{1-(r_i/r_c)^{24}} \quad (2)$$

Here n, r_i, and r_c denoted the calculated CN, the distance between the ith binding O and Cd(II), and the cutoff, respectively. In these simulations, r_c was 2.9 Å.

In each type of complex, the final configuration of the unconstrained simulation served as the initial input for the subsequent free energy calculation runs, and the initial configuration of every Q afterwards was based on the equilibrium geometry of the previous Q.

It was important to verify whether the hysteresis shown in the free-energy calculation (*e.g.* Ensing *et al.*, 2001) existed in the simulations. In addition to the route of the Cd(II) desorption process (the breakage of $Cd(II)-O_{surface}$), the free-energy calculation of the inverse process (adsorption) was also conducted for each complex, *i.e.* from outer-sphere complex to inner-sphere complex.

RESULTS

Equilibrium complexing structures

Stable Cd(II) complexes formed on the three binding sites in unconstrained simulations were shown in the snapshots (Figure 2), *i.e.* a monodentate complex formed on the $\equiv SiO$ site, a bidentate complex on the $\equiv Al(OH)_2$ site, and a tetradentate complex on the octahedral vacant site. These complex structures were very similar to the counterparts of Fe(II) that were found in previous FPMD studies (Liu *et al.*, 2013b, 2014). The complexes on the $\equiv SiO$ and $\equiv Al(OH)_2$ sites showed an octahedral configuration, with five and four water ligands, respectively (Figure 2a and 2b). For the complex on the octahedral vacancy, Cd(II) was coordinated with two water ligands and thus it presented a distorted octahedral geometry (Figure 2c). On the $\equiv SiO$ site, the length of the Cd(II)–O bond was 2.13 Å (Figure 2a), which was a little shorter than those bonds in the bidentate and tetradentate sites. This was due to the fact that the metal cation bonded with this dangling O more strongly than with the surface hydroxyls of the other two complexes. For the complex on the $\equiv Al(OH)_2$ site, the two binding OH were equivalent, and the two Cd(II)–O bonds were, therefore, almost the same, *i.e.* 2.20 Å and 2.21 Å (Figure 2b). For the complex on the vacant site, the $Cd(II)-O_{apical}$ bonds were obviously longer than the Cd(II)–OH bonds: the two $Cd(II)-O_{apical}$ bonds were identical (2.91 Å and 2.96 Å) and the two Cd(II)–OH bonds were identical (2.21 Å and 2.22 Å) as well (Figure 2c).

Free energy changes

The free-energy changes of Cd(II) complexes adsorbed on three complexing sites (Figure 3) showed

https://doi.org/10.1346/CCMN.2016.0640402 Published online by Cambridge University Press

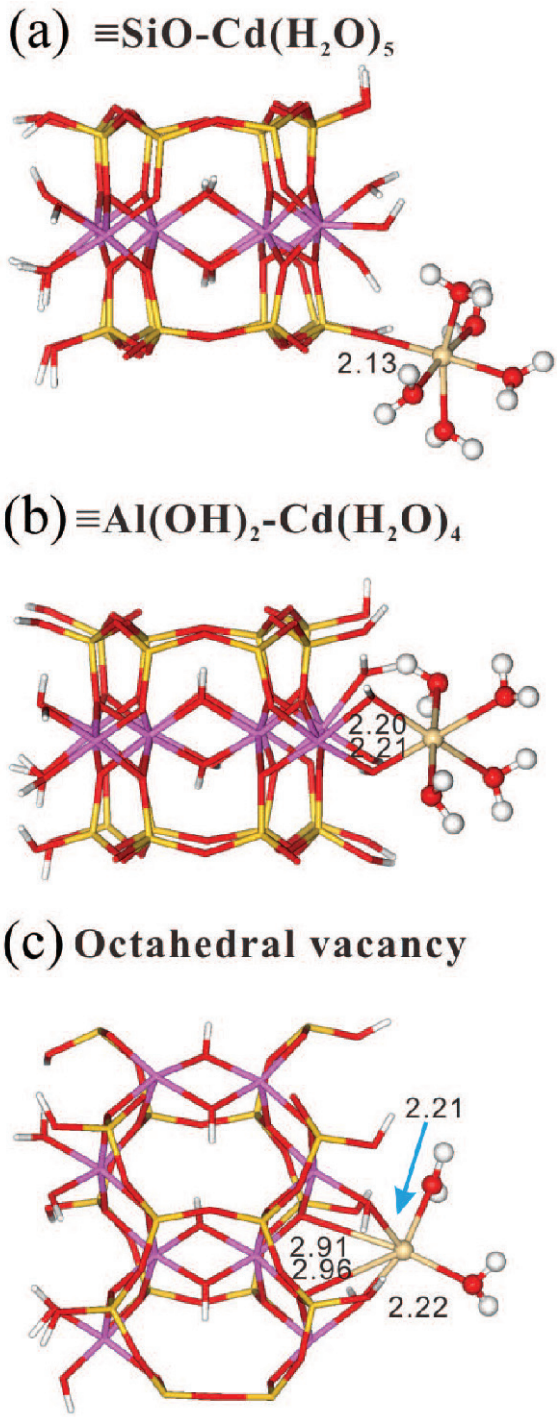


Figure 2. The equilibrium structures of Cd(II) complexes adsorbed on three binding sites on the (010) type interface of neutral framework 2:1 phyllosilicates. (a) ≡SiO site, (b) ≡$Al(OH)_2$ site, and (c) vacant site. For clarity, the other water molecules have been removed. Solid parts are shown as sticks; Cd(II) and the coordinated water molecules are shown as ball-and-stick models. O = red (black), H = white (white), Si = yellow (gray), Al = purple (dark gray), and Cd = gold (light gray) with grayscale in parentheses.

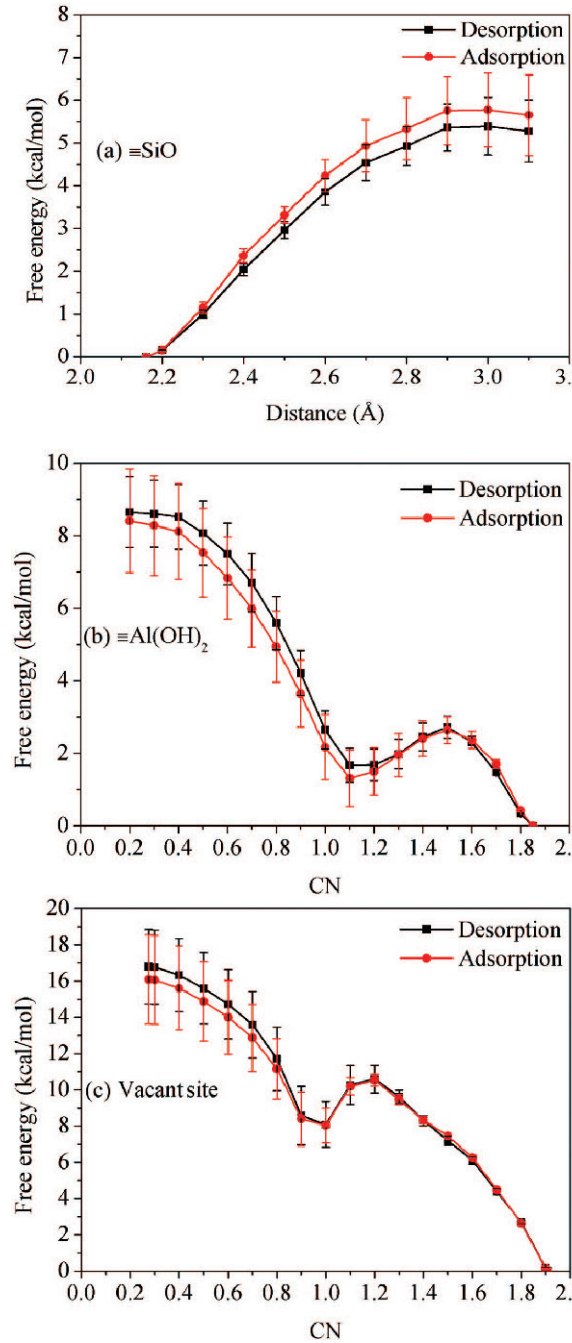


Figure 3. The calculated free-energy profiles for desorption and adsorption processes of Cd(II) complexes on (a) ≡SiO, (b) ≡$Al(OH)_2$, and (c) vacant site. The curves serve as a visual guide.

that the maximum difference between the two curves was only 0.7 kcal/mol (Figure 3c), which indicated that the hysteresis was within the error bars and negligible in these calculations. The free-energy changes for the desorption processes are summarized in Table 1.

For the complex ≡SiO−$Cd(H_2O)_5$, as shown by the free-energy profile (Figure 3a), the desorption free

https://doi.org/10.1346/CCMN.2016.0640402 Published online by Cambridge University Press

Table 1. Free-energy changes (in kcal/mol) for the desorption processes of three edge complexing sites.

Sites	ΔF
≡SiO	5.4 ± 0.7
≡$Al(OH)_2$	8.7 ± 1.0
Vacant site	16.8 ± 2.0

The statistical error of free energy is calculated by the thermodynamic integration relation (equation 1). The force of statistical error is the semi-difference between the force values using the first half and the second half of trajectory only.

energy was approximately 5.4 kcal/mol. The snapshots of the initial and final configurations derived from the constrained MD simulations were depicted for comparison (Figure 4). The Al(III) cation neighboring the SiO−Cd(II) complex was five-fold coordinated (Figure 4) because spontaneous desorption of the H_2O ligand happened in the equilibrium stage. This was also observed in a previous study (Liu *et al.*, 2012a). The structure at a distance of 2.1 Å (Figure 4a) was almost the same as the equilibrium structure of the free simulation. As the Cd(II)−O distance increased to 3.1 Å, the configuration was considered to mark the end of the desorption process where Cd(II) interacted with the ≡SiO group through hydrogen bonds (Figure 4b).

For the complex of Cd(II) adsorbed at the ≡$Al(OH)_2$ site, the desorption free energy was 8.7 kcal/mol. At CN = 1.9, the configuration of the complex (Figure 5a) was the same as the equilibrium structure where Cd(II) was coordinated with four water ligands. The free energy (black curve in Figure 3b) started to increase from CN = 1.85. The energy barrier at CN = 1.5 was ~2.7 kcal/mol. After that, free energy decreased to a local minimum of 1.7 kcal/mol (CN = 1.1). At this minimum, one of the ≡$Al(OH)_2$-Cd(II) bonds was broken and a solvent water molecule entered the solvation shell of Cd(II) (Figure 5b). From the local minimum at CN = 1.1 to CN = 0.2, the free energy change was 7.0 kcal/mol. This value was the energy to break a single ≡AlOH−Cd(II) bond. At CN = 0.1, the inner-sphere complex of Cd(II) was completely broken, and another solvent water molecule became the ligand of Cd(II). Thus, Cd(II) formed an outer-sphere complex on the ≡$Al(OH)_2$ site with six water ligands (Figure 5c).

Compared to the monodentate and bidentate complexes, the desorption of Cd(II) cation from the octahedral vacancy showed a free-energy change of 16.8 kcal/mol (see the black curve in Figure 3c). This value was much larger than the complexes on the other two sites, which indicated that the adsorption of Cd(II) on the vacant site was much stronger than on the ≡SiO and ≡$Al(OH)_2$ sites. Based on these calculated free-energy values, this study suggests that the vacant site can be assigned to HES and the other two to LES for the (010) terminations.

The structures at some noteworthy values of the reaction coordinates in the free-energy calculations (Figure 6) revealed the structure at CN = 1.9, where Cd(II) is coordinated with four surface O (includes two apical O and two OH groups connected to different Al(III) groups) and two water molecules (see the snapshot in Figure 6a) are used as the initial configuration. As CN gradually decreased, the free energy increased until CN = 1.2 and subsequently decreased slightly to a local minimum at CN = 1.0, and free energy continued to increase until the end (black curve in Figure 3c). The energy barrier at CN = 1.2 was about 11.0 kcal/mol. With the decrease of CN, Cd(II) first detached from the lower O_{AlOH} (see the snapshots in Figure 6a and 6b). When CN changed to 1.0, Cd(II) captured a water from the solvent and yielded a complex configuration of Cd(II) coordi-

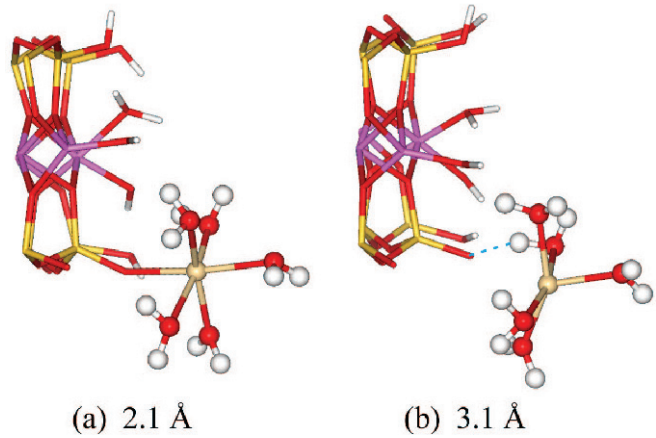


Figure 4. Snapshots of the free-energy calculation process of the Cd(II) complex on ≡SiO sites at distances (a) 2.1 Å and (b) 3.1 Å. For clarity, the other water molecules and substrates have been removed. The dotted line represents the hydrogen bond. Solid parts are shown as sticks; cations and coordinated water molecules are shown as ball-and-stick models.

https://doi.org/10.1346/CCMN.2016.0640402 Published online by Cambridge University Press

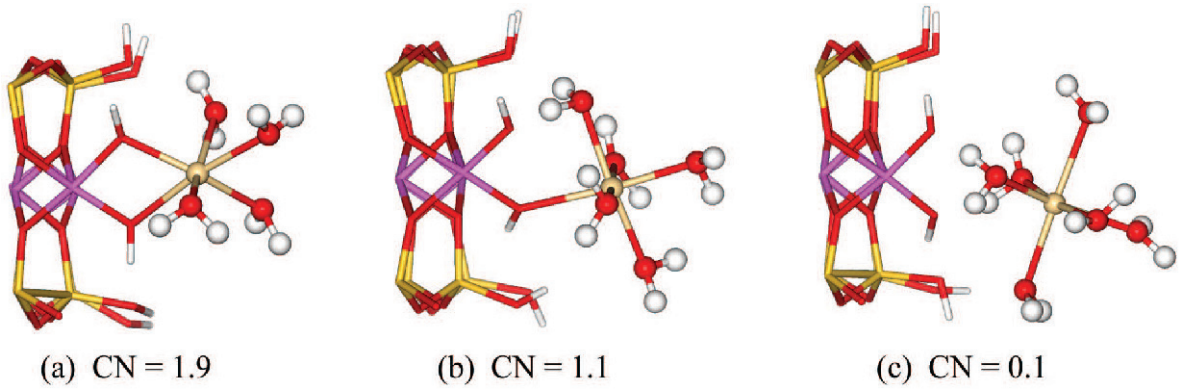


Figure 5. Snapshots of the free-energy calculation process of the Cd(II) complex on the $\equiv Al(OH)_2$ site at CN (a) 1.9, (b) 1.1, and (c) 0.1. For clarity, the other water molecules and substrates have been removed. Solid parts are shown as sticks; cations and the coordinated water molecules are shown as ball-and-stick models.

nated with an OH of the aluminol group and three water molecules (Figure 6b). At CN = 0.9, another water molecule bonded with Cd(II) and the complex, therefore, had four water ligands (Figure 6c). As CN decreased to 0.1, one of the solvent water molecules entered the solvation shell of Cd(II) and, therefore, caused Cd(II) to have five water ligands (Figure 6d). Combining these observations with the free-energy curve shown above (Figure 3c), the last structure was considered as the end of the desorption process. The free-energy value from local minimum (CN = 1.0) to the end (approximately at CN = 0.28) was 8.7 kcal/mol (Figure 3c), which was identified as the energy to break a single Cd(II)−OH bond. This value was similar to the energy needed to break the bidentate complex (7.0 kcal/mol).

DISCUSSION

In this study, the model had four vacant sites, four bidentate $\equiv Al(OH)_2$ sites, and eight monodentate $\equiv SiO$ sites; hence, the ratio of HES to LES was 1:3. This was different from the assumption used in the 2 SPNESC/CE model (1:20) (Bradbury and Baeyens, 1997). One can see a qualitative consistency in both models in that HES were significantly less than LES, but to reach a full agreement was impossible. First, the complexity of clay surfaces, such as the high heterogeneity of broken surfaces and very similar bond lengths of different surface groups, making the use of an experimental method to accurately quantify different surface sites difficult. The estimates of Bradbury and Baeyens (1997) were derived from sorption isotherms, but they had no microscopic basis. On the other hand, the present model was a periodic surface cut from the unit cell but neglected the fact that clay particles commonly occur with diverse surfaces. This model was used to represent the complexing structures and free energies, but it cannot exactly reflect the real surface site capacities of clay particles. This issue definitely deserves more experimental and theoretical studies in the future.

The equilibrium structures of complexes adsorbed on the three possible sites on (110) terminations have also been derived for comparison: a monodentate complex on the $\equiv SiO$ site, a bidentate complex on the

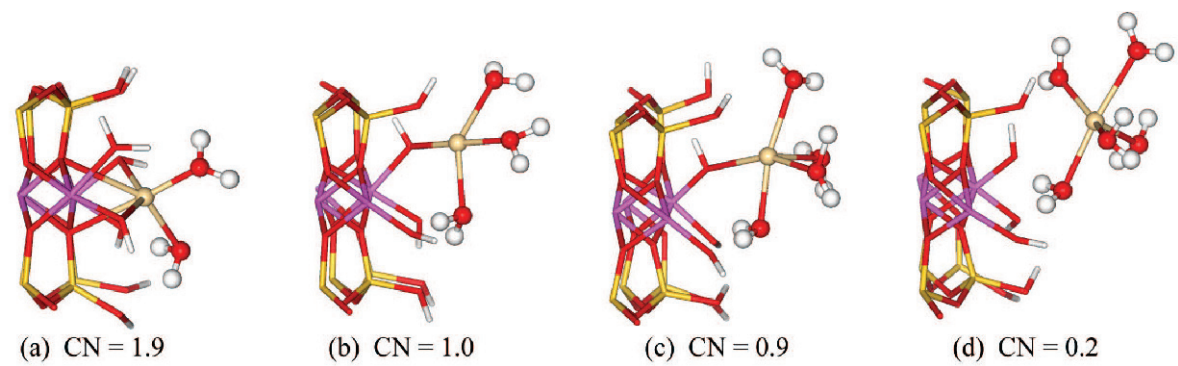


Figure 6. Snapshots of the free-energy calculation process of the Cd(II) complex on the vacant site at CN (a) 1.9, (b) 1.0, (c) 0.9, and (d) 0.2. For clarity, the other water molecules and substrates have been removed, and one OH_2 ligand of edge Al(III) has been removed in (b), (c), and (d). Solid parts are shown as sticks; cations and the coordinated water molecules are shown as ball-and-stick models.

https://doi.org/10.1346/CCMN.2016.0640402 Published online by Cambridge University Press

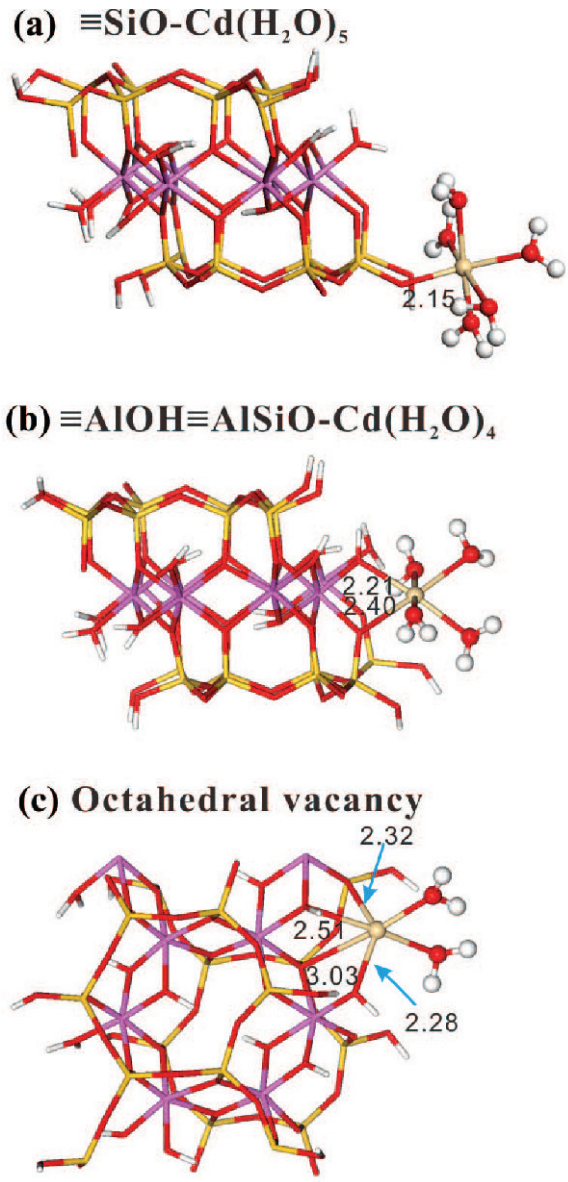


Figure 7. The equilibrium structures of Cd(II) complexes adsorbed on three binding sites on (110) type interface of the neutral framework of 2:1 phyllosilicates. (a) ≡SiO site, (b) ≡AlOH≡AlSiO site, and (c) vacant site. For clarity, the other water molecules have been removed. Solid parts are shown as sticks; Cd(II) and its coordinated waters are shown as ball-and-stick models.

≡AlOH≡AlSiO site, and a tetradentate complex on the octahedral vacant site (Figure 7).

For the ≡Si−O sites, the two complexes were very similar (see the snapshots in Figures 2a and 7a) and the two Cd(II)-O bonds had similar lengths (2.13 Å *vs.* 2.15 Å). The free energy of the complex on this site was thus assumed to be similar to that on the (010) edge. For the complex on the ≡AlOH≡AlSiO site on the (110) surface the ≡AlOH−Cd(II) bond was similar to the ≡AlOH−Cd(II) bonds on the (010) surface (2.21 Å *vs.* 2.20 Å and 2.21 Å, in Figures 2b and 7b), which was a little shorter than the Cd−O_{apical} bond (2.40 Å, in Figure 7b). This originated from the fact that the apical O was a poor acceptor of protons (the ≡AlSi(OH) site had a rather low pKa of 1.7) (Liu *et al.*, 2014). The ≡AlSiO has also been demonstrated to be less reactive compared to the other surface groups (Churakov, 2007). The observations on bond lengths suggested that the free energy of the bidentate complex on the ≡AlOH≡AlSiO site on the (110) surface was lower than that of ≡$Al(OH)_2$−Cd on the (010) surface. The energy to break the ≡AlOH−Cd(II) bond was supposed to be close to that required to break the ≡AlOH−Cd(II) bond on the (010) surface. Then the free energy of this bidentate complex must be still larger than 7.0 kcal/mol (one ≡AlOH−Cd(II) bond strength). For the complex on the vacant site, one of the Cd(II)−O_{inner} bond lengths was 2.51 Å and the other was 3.03 Å. The Cd(II)−O_{outer} bond lengths (2.32 Å and 2.28 Å in Figure 7c) were a little longer than those on the (010) surface (2.21 Å and 2.22 Å, in Figure 2c). The free energy of this complex was thus expected to be less than that of the tetradentate complex on the (010) edge surface (16.8 kcal/mol), but undoubtedly this value should be significantly >8.7 kcal/mol (one ≡AlOH−Cd(II) bond strength). For the (110) edge surface, therefore, the monodentate and bidentate complexes should have similar free energies, and they were both significantly less than that of the tetradentate complex. Similar to the (010) surface, the vacant complexing site was assigned to HES and the other two sites (≡SiO and ≡AlOH≡AlSiO) to LES.

For other divalent heavy metal cations, such as Ni(II), Zn(II), Co(II), Fe(II), and Cu(II), the pH-dependent adsorption on edge surfaces of 2:1 phyllosilicates in aqueous solutions were very similar. The stable complexes of Cd(II) adsorbed on the (010) and (110) terminations in the present study agreed with the complexes of Fe(II) in previous reports (Liu *et al.*, 2013b, 2014). This indicated that other divalent heavy metal cations may form similar complexes as illustrated above (Figures 2 and 7). The complexes of these cations on the ≡SiO and the ≡$Al(OH)_2$/≡AlOH≡AlSiO sites were, therefore, likely to have similar free-energy values, and these values were supposed to be obviously less than those of the complexes on vacant sites. Similar to the case of Cd(II) for these heavy metal cations, the vacant site may also be assigned to HES and the ≡SiO and ≡$Al(OH)_2$/≡AlOH≡AlSiO sites to LES. Churakov and Dähn (2012) claimed that Zn was incorporated into the outermost octahedra at low loading. In fact, the complex structures on incorporation sites in their report were very similar to those of Cd(II) on vacant sites, *i.e.* cations bonded with four O/OH of the substrates and two OH/OH_2 ligands. One could, therefore, reasonably deduce that the complexes on these two sites have similar free energies.

https://doi.org/10.1346/CCMN.2016.0640402 Published online by Cambridge University Press

CONCLUSIONS

By using FPMD simulations, the stable complexes of Cd(II) adsorbed on (010) and (110) interfaces of a neutral 2:1 phyllosilicate framework (*i.e.* pyrophyllite) [Talc is different from our model] were derived. For the (010) surface, the $\equiv$SiO, $\equiv$Al(OH)$_2$, and octahedral vacant sites and for the (110) surface, the $\equiv$SiO, $\equiv$AlOH$\equiv$AlSiO, and vacant octahedral sites were investigated. The structures of complexes on each site were similar for the two surfaces, *i.e.* monodentate complexes on the $\equiv$SiO sites, bidentate complexes on the $\equiv$Al(OH)$_2$ site/$\equiv$AlOH$\equiv$AlSiO sites, and tetradentate complexes on the vacant sites. For the (010) surface, the constrained FPMD method was employed to calculate the desorption/adsorption free energy for each complex. The free energies of the complexes on the $\equiv$SiO and $\equiv$Al(OH)$_2$ sites were similar and were obviously less than that of the complex on the vacant octahedral site. The octahedral vacancy and the other two sites, therefore, can be respectively assigned to HES and LES for the (010) terminations. The same situation was also inferred for the (110) terminations. This conclusion is likely to be applicable to other divalent heavy metal cations on the basis of the fact that other divalent heavy metal cations have pH-dependent adsorption behaviors and complexing structures that are similar to Cd(II). This work provides a thermodynamic basis for the HES and LES on the edges of clay minerals. The calculated atomic-level structures and free-energy values can be used for further understanding the interfacial chemistry of phyllosilicates.

ACKNOWLEDGMENTS

The authors acknowledge the National Science Foundation of China (Nos. 41222015, 41273074, 41425009, and 41572027), the Foundation for the Author of National Excellent Doctoral Dissertation of PR China (No. 201228), Special Program for Applied Research on Super Computation of the NSFC-Guangdong Joint Fund (the second phase), the Newton International Fellow Program, and financial support from the State Key Laboratory for Mineral Deposits Research. The authors thank Prof. Andrey Kalinichev and Dr. Zongyuan Chen for fruitful discussions. They are also grateful to the High Performance Computing Center of Nanjing University for use of the IBM Blade cluster system.

REFERENCES

Alexandrov, V. and Rosso, K.M. (2013) Insights into the mechanism of Fe(II) adsorption and oxidation at Fe-clay mineral surfaces from first-principles calculations. *Journal of Physical Chemistry C*, **117**, 22880–22886.

Anderson, R.L., Ratcliffe, I., Greenwell, H.C., Williams, P.A., Cliffe, S., and Coveney, P.V. (2010) Clay swelling - a challenge in the oilfield. *Earth-Science Reviews*, **98**, 201–216.

Baeyens, B. and Bradbury, M.H. (1997) A mechanistic description of Ni and Zn sorption on Na-montmorillonite. 1. Titration and sorption measurements. *Journal of Contaminant Hydrology*, **27**, 199–222.

Barbier, F., Duc, G., and Petit-Ramel, M. (2000) Adsorption of lead and cadmium ions from aqueous solution to the montmorillonite/water interface. *Colloids and Surfaces A: Physicochemical and Engineering Aspects*, **166**, 153–159.

Bergaya, F. and Lagaly, G. (2013) General introduction: Clays, clay minerals, and clay science. Ch. 1. Pp. 1–19 in: *Handbook of Clay Science* (F. Bergaya and G. Lagaly, editors). Developments in Clay Science, **5A**. Elsevier.

Bickmore, B.R., Rosso, K.M., Nagy, K.L., Cygan, R.T., and Tadanier, C.J. (2003) Ab initio determination of edge surface structures for dioctahedral 2:1 phyllosilicates: Implications for acid-base reactivity. *Clays and Clay Minerals*, **51**, 359–371.

Bleam, W.F. (1993) Atomic theories of phyllosilicates-quantum-chemistry, statistical-mechanics, electrostatic theory, and crystal-chemistry. *Reviews of Geophysics*, **31**, 51–73.

Boek, E.S. and Sprik, M. (2003) Ab initio molecular dynamics study of the hydration of a sodium smectite clay. *Journal of Physical Chemistry B*, **107**, 3251–3256.

Boulet, P., Greenwell, H.C., Stackhouse, S., and Coveney, P.V. (2006) Recent advances in understanding the structure and reactivity of clays using electronic structure calculations. *Journal of Molecular Structure-Theochem*, **762**, 33–48.

Bradbury, M.H. and Baeyens, B. (1997) A mechanistic description of Ni and Zn sorption on Na-montmorillonite. 2. Modelling. *Journal of Contaminant Hydrology*, **27**, 223–248.

Bradbury, M.H. and Baeyens, B. (1999) Modelling the sorption of Zn and Ni on Ca-montmorillonite. *Geochimica et Cosmochimica Acta*, **63**, 325–336.

Bradbury, M.H. and Baeyens, B. (2005a) Modelling the sorption of Mn(II), Co(II), Ni(II), Zn(II), Cd(II), Eu(III), Am(III), Sn(IV), Th(IV), Np(V) and U(VI) on montmorillonite: linear free energy relationships and estimates of surface binding constants for some selected heavy metals and actinides. *Geochimica et Cosmochimica Acta*, **69**, 875–892.

Bradbury, M.H. and Baeyens, B. (2005b) Experimental measurements and modeling of sorption competition on montmorillonite. *Geochimica et Cosmochimica Acta*, **69**, 4187–4197.

Bradbury, M.H., Baeyens, B., Geckeis, H., and Rabung, T. (2005) Sorption of Eu(III)/Cm(III) on Ca-montmorillonite and Na-illite. Part 2: Surface complexation modelling. *Geochimica et Cosmochimica Acta*, **69**, 5403–5412.

Brindley, G.W. and Brown, G. (editors) (1980) *Crystal Structures of Clay Minerals and their X-ray Identification*. Mineralogical Society Monograph **5**, London.

Brigatti, M.F., Galán, E., and Theng, B.K.G. (2013) Structure and mineralogy of clay minerals. Pp. 21–81 in: *Handbook of Clay Science* (F. Bergaya and G. Lagaly, editors). Developments in Clay Science, **5A**. Elsevier.

Car, R. and Parrinello, M. (1985) Unified approach for molecular-dynamics and density-functional theory. *Physical Review Letters*, **55**, 2471–2474.

Carter, E.A., Ciccotti, G., Hynes, J.T., and Kapral, R. (1989) Constrained reaction coordinate dynamics for the simulation of rare events. *Chemical Physics Letters*, **156**, 472–477.

Churakov, S.V. (2007) Structure and dynamics of the water films confined between edges of pyrophyllite: a first principle study. *Geochimica et Cosmochimica Acta*, **71**, 1130–1144.

Churakov, S.V. and Kosakowski, G. (2010) An ab initio molecular dynamics study of hydronium complexation in Na-montmorillonite. *Philosophical Magazine*, **90**, 2459–2474.

Churakov, S.V. and Dähn, R. (2012) Zinc adsorption on clays

https://doi.org/10.1346/CCMN.2016.0640402 Published online by Cambridge University Press

inferred from atomistic simulations and EXAFS spectroscopy. *Environmental Science & Technology*, **46**, 5713–5719.

Cygan, R.T., Greathouse, J.A., Heinz, H., and Kalinichev, A.G. (2009) Molecular models and simulations of layered materials. *Journal of Materials Chemistry*, **19**, 2470.

Dähn, R., Scheidegger, A.M., Manceau, A., Schlegel, M.L., Baeyens, B., Bradbury, and M.H., Chateigner, D. (2003) Structural evidence for the sorption of Ni(II) atoms on the edges of montmorillonite clay minerals: a polarized X-ray absorption fine structure study. *Geochimica et Cosmochimica Acta*, **67**, 1–15.

Dähn, R., Baeyens, B., and Bradbury, M.H. (2011) Investigation of the different binding edge sites for Zn on montmorillonite using P-EXAFS - the strong/weak site concept in the 2SPNE SC/CE sorption model. *Geochimica et Cosmochimica Acta*, **75**, 5154–5168.

Davis, J.A. and Kent, D.B. (1990) Surface complexation modeling in aqueous geochemistry. Pp. 177–260 in: *Mineral-Water Interface Geochemistry* (M.F. Hochella and A.F. White, editors). Reviews in Mineralogy, **23**. Mineralogical Society of America, Chantilly, Virginia, USA.

Ensing, B., Meijer, E.J., Blochl, P.E., and Baerends, E.J. (2001) Solvation effects on the S(N)2 reaction between CH3Cl and Cl- in water. *Journal of Physical Chemistry A*, **105**, 3300–3310.

Evans, L.J. (1989) Chemistry of metal retention by soils - several processes are explained. *Environmental Science & Technology*, **23**, 1046–1056.

Gaines, G.L. and Thomas, H.C. (1953) Adsorption studies on clay minerals. II. A formulation of the thermodynamics of exchange adsorption. *Journal of Chemical Physics*, **21**, 714–718.

Geckeis, H., Luetzenkirchen, J., Polly, R., Rabung, T., and Schmidt, M. (2013) Mineral-water interface reactions of actinides. *Chemical Reviews*, **113**, 1016–1062.

Goedecker, S., Teter, M., and Hutter, J. (1996) Separable dual-space Gaussian pseudopotentials. *Physical Review B*, **54**, 1703–1710.

Gu, X. and Evans, L.J. (2008) Surface complexation modelling of Cd(II), Cu(II), Ni(II), Pb(II) and Zn(II) adsorption onto kaolinite. *Geochimica et Cosmochimica Acta*, **72**, 267–276.

Gu, X., Evans, L.J., and Barabash, S.J. (2010) Modeling the adsorption of Cd (II), Cu (II), Ni (II), Pb (II) and Zn (II) onto montmorillonite. *Geochimica et Cosmochimica Acta*, **74**, 5718–5728.

Gu, X., Sun, J., and Evans, L.J. (2014) The development of a multi-surface soil speciation model for Cd (II) and Pb (II): comparison of two approaches for metal adsorption to clay fractions. *Applied Geochemistry*, **47**, 99–108.

Ikhsan, J., Wells, J.D., Johnson, B.B., and Angove, M.J. (2005) Surface complexation modeling of the sorption of Zn(II) by montmorillonite. *Colloids and Surfaces A-Physicochemical and Engineering Aspects*, **252**, 33–41.

Jo, H.Y., Benson, C.H., and Edil, T.B. (2006) Rate-limited cation exchange in thin bentonitic barrier layers. *Canadian Geotechnical Journal*, **43**, 370–391.

Kremleva, A., Krueger, S., and Roesch, N. (2009) Uranyl adsorption at solvated (010) edge surfaces of kaolinite. *Abstracts of Papers of the American Chemical Society*, **237**.

Kremleva, A., Krueger, S., and Roesch, N. (2011) Uranyl adsorption at (010) edge surfaces of kaolinite: a density functional study. *Geochimica et Cosmochimica Acta*, **75**, 706–718.

Kremleva, A., Martorell, B., Krueger, S., and Roesch, N. (2012) Uranyl adsorption on solvated edge surfaces of pyrophyllite: a DFT model study. *Physical Chemistry Chemical Physics*, **14**, 5815–5823.

Kremleva, A., Krueger, S., and Roesch, N. (2015) Uranyl adsorption at solvated edge surfaces of 2:1 smectites. A density functional study. *Physical Chemistry Chemical Physics*, **17**, 13757–13768.

Kubicki, J.D., Kwon, K.D., Paul, K.W., and Sparks, D.L. (2007) Surface complex structures modelled with quantum chemical calculations: carbonate, phosphate, sulphate, arsenate and arsenite. *European Journal of Soil Science*, **58**, 932–944.

Lagaly, G. and Dékány, I., (2013) Colloid clay science. Pp. 243–345 in: *Handbook of Clay Science* (F. Bergaya and G. Lagaly, editors). Developments in Clay Science, **5A**. Elsevier.

Lippert, G., Hutter, J., and Parrinello, M. (1997) A hybrid Gaussian and plane wave density functional scheme. *Molecular Physics*, **92**, 477–487.

Liu, X. and Lu, X. (2006) A thermodynamic understanding of clay-swelling inhibition by potassium ions. *Angewandte Chemie*, **45**, 6300–6303.

Liu, X., Lu, X., Wang, R., and Zhou, H. (2008) Effects of layer-charge distribution on the thermodynamic and microscopic properties of Cs-smectite. *Geochimica et Cosmochimica Acta*, **72**, 1837–1847.

Liu, X., Lu, X., Wang, R., Meijer, E.J., and Zhou, H. (2011) Acidities of confined water in interlayer space of clay minerals. *Geochimica et Cosmochimica Acta*, **75**, 4978–4986.

Liu, X., Lu, X., Meijer, E.J., Wang, R., and Zhou, H. (2012a) Atomic-scale structures of interfaces between phyllosilicate edges and water. *Geochimica et Cosmochimica Acta*, **81**, 56–68.

Liu, X., Lu, X., Wang, R., Meijer, E.J., Zhou, H., and He, H. (2012b) Atomic scale structures of interfaces between kaolinite edges and water. *Geochimica et Cosmochimica Acta*, **92**, 233–242.

Liu, X., Meijer, E.J., Lu, X., and Wang, R. (2012c) First-principles molecular dynamics insight into Fe^{2+} complexes adsorbed on edge surfaces of clay minerals. *Clays and Clay Minerals*, **60**, 341–347.

Liu, X., Cheng, J., Sprik, M., Lu, X., and Wang, R. (2013a) Understanding surface acidity of gibbsite with first principles molecular dynamics simulations. *Geochimica et Cosmochimica Acta*, **120**, 487–495.

Liu, X., Lu, X., Sprik, M., Cheng, J., Meijer, E.J., and Wang, R. (2013b) Acidity of edge surface sites of montmorillonite and kaolinite. *Geochimica et Cosmochimica Acta*, **117**, 180–190.

Liu, X., Cheng, J., Sprik, M., Lu, X., and Wang, R. (2014) Surface acidity of 2:1-type dioctahedral clay minerals from first principles molecular dynamics simulations. *Geochimica et Cosmochimica Acta*, **140**, 410–417.

Martorell, B., Kremleva, A., Krueger, S., and Roesch, N. (2010) Density functional model study of uranyl adsorption on the solvated (001) surface of kaolinite. *Journal of Physical Chemistry C*, **114**, 13287–13294.

Marx, D. and Hutter, J. (2009) *Ab initio Molecular Dynamics – Basic Theory and Advance Methods*. Cambridge University Press, Cambridge, UK.

Mooney, R.W., Keenan, A.G., and Wood, L.A. (1952) Adsorption of water vapor by montmorillonite. II. Effect of exchangeable ions and lattice swelling as measured by X-ray diffraction. *Journal of the American Chemical Society*, **74**,1367–1371.

Perdew, J.P., Burke, K., and Ernzerhof, M. (1996) Generalized gradient approximation made simple. *Physical Review Letters*, **77**, 3865–3868.

Pye, C.C., Tomney, M.R., and Rudolph, W.W. (2006) Cadmium hydration: hexacoordinate or heptacoordinate? *Canadian Journal of Analytical Sciences and Spectroscopy*, **51**, 140–146.

https://doi.org/10.1346/CCMN.2016.0640402 Published online by Cambridge University Press

Rudolph, W.W. and Pye, C.C. (1998) Raman spectroscopic measurements and ab initio molecular orbital studies of cadmium(II) hydration in aqueous solution. *Journal of Physical Chemistry B*, **102**, 3564–3573.

Schlegel, M.L. and Manceau, A. (2013) Binding mechanism of Cu(II) at the clay-water interface by powder and polarized EXAFS spectroscopy. *Geochimica et Cosmochimica Acta*, **113**, 113–124.

Schoonheydt, R.A. and Johnston, C.T. (2013) Surface and interface chemistry of clay minerals. Pp. 139–172 in: *Handbook of Clay Science* (F. Bergaya and G. Lagaly, editors). Developments in Clay Science, **5A**. Elsevier.

Soltermann, D., Baeyens, B., Bradbury, M.H., and Fernandes, M.M. (2014) Fe(II) uptake on natural montmorillonites. II. Surface complexation modeling. *Environmental Science & Technology*, **48**, 8698–8705.

Sposito, G. (1984) *The Surface Chemistry of Soils*. Oxford University Press, New York.

Sposito, G., Skipper, N.T., Sutton, R., Park, S.H., Soper, A.K., and Greathouse, J.A. (1999) Surface geochemistry of the clay minerals. *Proceedings of the National Academy of Sciences of the United States of America*, **96**, 3358–3364.

Sprik, M. (1998) Coordination numbers as reaction coordinates in constrained molecular dynamics. *Faraday Discussions*, **110**, 437–445.

Sprik, M. and Ciccotti, G. (1998) Free energy from constrained molecular dynamics. *Journal of Chemical Physics*, **109**, 7737–7744.

Sprik, M. (2000) Computation of the pK of liquid water using coordination constraints. *Chemical Physics*, **258**, 139–150.

Tournassat, C., Grangeon, S., Leroy, P., and Giffaut, E. (2013) Modeling specific pH dependent sorption of divalent metals on montmorillonite surfaces. A review of pitfalls, recent achievements and current challenges. *American Journal of Science*, **313**, 395–451.

Tunega, D., Gerzabek, M.H., and Lischka, H. (2004) Ab initio molecular dynamics study of a monomolecular water layer on octahedral and tetrahedral kaolinite surfaces. *Journal of Physical Chemistry B*, **108**, 5930–5936.

Turner, D.R., Bertetti, F.P., and Pabalan, R.T. (2006) Applying surface complexation modeling to radionuclide sorption. Pp. 553–604 in: *Interface Science and Technology* (L. Johannes, editor). Elsevier.

VandeVondele, J., Krack, M., Mohamed, F., Parrinello, M., Chassaing, T., and Hutter, J. (2005) QUICKSTEP: Fast and accurate density functional calculations using a mixed Gaussian and plane waves approach. *Computer Physics Communications*, **167**, 103–128.

Viani, A., Gaultieri, A.F., and Artioli, G. (2002) The nature of disorder in montmorillonite by simulation of X-ray powder patterns. *American Mineralogist*, **87**, 966–975.

Wagner, J.F. (2013) Clay liners and waste disposal. Pp. 663–676 in: *Handbook of Clay Science* (F. Bergaya and G. Lagaly, editors). Developments in Clay Science, **5A**. Elsevier.

White, G.N. and Zelazny, L.W. (1988) Analysis and implications of the edge structure of dioctahedral phyllosilicates. *Clays and Clay Minerals*, **36**, 141–146.

Yuan, G.D., Theng, B.K.G., Churchman, G.J., and Gates, W.P. (2013) Clays and clay minerals for pollution control. Pp. 587–644. in: *Handbook of Clay Science* (F. Bergaya and G. Lagaly, editors). Developments in Clay Science, **5A**. Elsevier.

Zachara, J.M., Smith, S.C., McKinley, J.P., and Resch, C.T. (1993) Cadmium sorption on specimen and soil smectites in sodium and calcium electrolytes. *Soil Science Society of America Journal*, **57**, 1491–1501.

Zachara, J.M. and Smith, S.C. (1994) Edge complexation reactions of cadmium on specimen and soil-derived smectite. *Soil Science Society of America Journal*, **58**, 762–769.

(*Received 16 September 2015; revised 9 March 2016; Ms. 1034; AE: A.G. Kalinichev*)

https://doi.org/10.1346/CCMN.2016.0640402 Published online by Cambridge University Press